iScience

CellPress
OPEN ACCESS

Article

Optokinetic set-point adaptation functions as an internal dynamic calibration mechanism for oculomotor disequilibrium

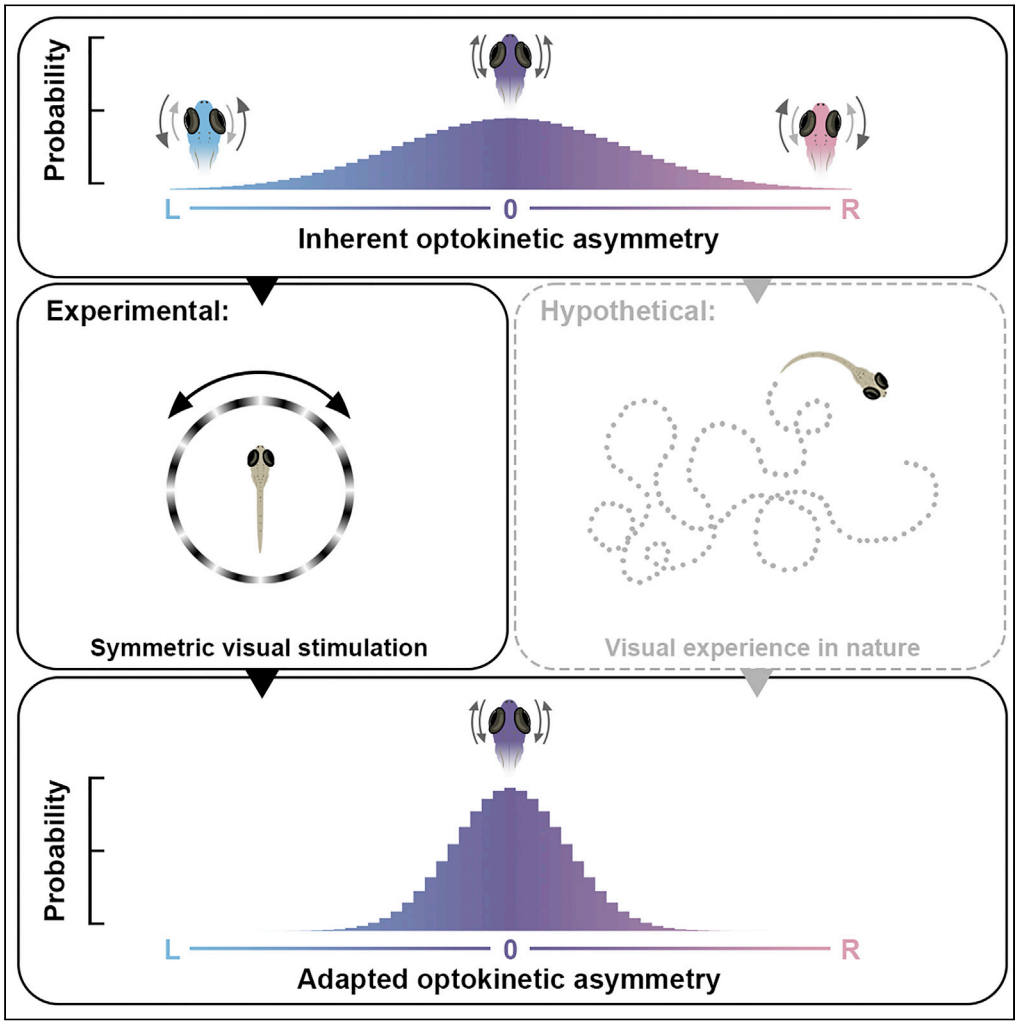

Ting-Feng Lin, Mohammad Mohammadi, Kathleen E. Cullen, Maurice J. Chacron, Melody Ying-Yu Huang

tingfenglin.ac@gmail.com (T.-F.L.)
melody.yingyu.huang@gmail.com (M.Y.-Y.H.)

Highlights

Optokinetic set-point adaptation reflects the temporal integration of visual input

Wild-type zebrafish larvae may display innate optokinetic left-right asymmetries

The degree of the optokinetic asymmetry among larvae is normally distributed

The innate optokinetic asymmetry can be compensated by the set-point adaptation

Lin et al., iScience 25, 105335
November 18, 2022 © 2022 The Authors.
https://doi.org/10.1016/j.isci.2022.105335

iScience

CellPress
OPEN ACCESS

Article

Optokinetic set-point adaptation functions as an internal dynamic calibration mechanism for oculomotor disequilibrium

Ting-Feng Lin,[1,2,9,13,*] Mohammad Mohammadi,[3] Kathleen E. Cullen,[4,5,6,7] Maurice J. Chacron,[8] and Melody Ying-Yu Huang[1,2,10,11,12,*]

SUMMARY

Experience-dependent brain circuit plasticity underlies various sensorimotor learning and memory processes. Recently, a novel set-point adaptation mechanism was identified that accounts for the pronounced negative optokinetic afternystagmus (OKAN) following a sustained period of unidirectional optokinetic nystagmus (OKN) in larval zebrafish. To investigate the physiological significance of optokinetic set-point adaptation, animals in the current study were exposed to a direction-alternating optokinetic stimulation paradigm that better resembles their visual experience in nature. Our results reveal that not only was asymmetric alternating stimulation sufficient to induce the set-point adaptation and the resulting negative OKAN, but most strikingly, under symmetric alternating stimulation some animals displayed an inherent bias of the OKN gain in one direction, and that was compensated by the similar set-point adaptation. This finding, supported by mathematical modeling, suggests that set-point adaptation allows animals to cope with asymmetric optokinetic behaviors evoked by either external stimuli or innate oculomotor biases.

INTRODUCTION

Neural development is organized according to several levels of regulatory mechanisms. Although genetically coded chemoaffinity cues are important for the large-scale organization of neuronal projections, fine tuning of neural circuits requires activity-dependent plasticity in response to real-life experience (Cline, 2003). Before the onset of vestibular function in zebrafish during early development (Beck et al., 2004; Bever and Fekete, 2002; Lambert et al., 2008), freely swimming larvae largely rely on their visual system. Owing to technological advancements, larval zebrafish have evolved into an excellent model organism for studying neural circuitry related to visuomotor learning and control (Bollmann, 2019; Xie et al., 2019). A novel optokinetic set-point adaptation identified recently in larval zebrafish may reflect a visual experience-dependent eye movement adjusting mechanism (Lin et al., 2019); however, its physiological function remains unclear. Optokinetic nystagmus (OKN) is an eye-tracking behavior that uses a large moving field to stabilize images on the retina. OKN consists of both eye tracking and eye position resetting, i.e., slow phase and quick phase, respectively. Negative optokinetic afternystagmus (OKAN), on the other hand, is an eye movement aftereffect in which the eyes move in the opposite direction of the previous OKN. Studies conducted in various animal species have shown that an optokinetic stimulation period of longer than a minute is required to elicit negative OKAN (Barmack and Nelson, 1987; Buttner et al., 1976; Hess et al., 1985; Lin et al., 2019; Waespe et al., 1978). After two days of unidirectional stimulation, negative OKAN can last for up to 1-4 days in rabbits (Barmack and Nelson, 1987).

In our previous study, we established an underlying optokinetic set-point adaptation mechanism that can be accounted for the subsequent negative OKAN. Briefly, the optokinetic system exerts a negative-feedback control to reduce the error between retinal slip velocity and its set point by commanding the tracking eye movements. The default set point is about 0 deg/sec without previous visual stimulation, and to stabilize moving images on the retina, the retinal slip velocity should be reduced to zero. However, persisting optokinetic stimulation in one direction creates a sustained error signal that with time leads to the set-point adjustment to dampen the continuous eye-tracking movement. As a

[1]Department of Neurology, University Hospital Zurich, University of Zurich, Zurich, Switzerland

[2]Neuroscience Center Zurich (ZNZ), University of Zurich and ETH Zurich, Zurich, Switzerland

[3]Department of Biomedical Engineering, McGill University, Montreal, QC, Canada

[4]Department of Biomedical Engineering, The Johns Hopkins University, Baltimore, MD, USA

[5]Department of Otolaryngology-Head and Neck Surgery, Johns Hopkins University School of Medicine, Baltimore, MD, USA

[6]Department of Neuroscience, Johns Hopkins University School of Medicine, Baltimore, MD, USA

[7]Kavli Neuroscience Discovery Institute, The Johns Hopkins University, Baltimore, MD, USA

[8]Department of Physiology, McGill University, Montreal, QC, Canada

[9]Present address: Department of Neurobiology, The University of Chicago, Chicago, Illinois, USA

[10]Present address: Department of Health Sciences and Technology, Swiss Federal Institute of Technology (ETH) Zürich, Zürich, Switzerland

[11]Present address: Department for BioMedical Research, University of Bern, Bern, Switzerland

[12]Present address: Department of Anaesthesiology and Pain Medicine, Inselspital, Bern

Continued

This is an open access article under the CC BY-NC-ND license (http://creativecommons.org/licenses/by-nc-nd/4.0/).

result, when the stimulus is abruptly removed, the current non-zero set point simultaneously generates a new error signal with a reversed sign of the previous stimulus that results in negative OKAN (Lin et al., 2019).

In most of the previous investigations of negative OKAN, the behavior was induced by a prolonged period of unidirectional optokinetic stimulation (Barmack and Nelson, 1987; Brandt et al., 1974; Bures and Neverov, 1979; Buttner et al., 1976; Hess et al., 1985; Igarashi et al., 1983; Maioli, 1988; Neverov et al., 1977; Perez-Schuster et al., 2016; Waespe and Henn, 1977, 1978; Waespe and Wolfensberger, 1985; Wu et al., 2020). Such study designs are far from animals' visual experience during natural exploration. Since a persistent unidirectional optokinetic stimulus is not common outside the laboratory, it remains unclear what the physiological relevance of the optokinetic set-point adaptation is in everyday life. On the other hand, freely swimming larval zebrafish demonstrated spontaneous turning behaviors that consist of alternating states in which fish repeatedly turned in one direction before switching to the other (Dunn et al., 2016). Thus, in accordance with their swimming patterns, in the current study, we investigated OKN and negative OKAN under a direction-alternating optokinetic stimulation paradigm with the aim of developing a comprehensive understanding of the set-point adaptation and its functional significance in animals.

Specifically, the set-point adaptation was measured under prolonged optokinetic stimulation, with the direction alternating every 15 s. Moreover, we studied the OKN and the subsequent OKAN by applying both symmetric and asymmetric stimulus velocities in different directions. Our results revealed that prolonged asymmetric direction-alternating optokinetic stimulation was sufficient to induce the optokinetic set-point adaptation and the resulting negative OKAN in darkness, which further suggests that the adaptation is a consequence of temporal integration and not an instantaneous effect of the visual experience. Most strikingly, the results showed that symmetric stimulation could lead to negative OKAN in individual larvae that inherently displayed asymmetric OKN gains in different directions. Ultimately, our mathematical model predicts that innate OKN biases will result in set-point adaptation and the subsequent negative OKAN. Thus, our study suggests that the functional relevance of the set-point adaptation is to adjust the inherent oculomotor disequilibrium in the optokinetic system.

RESULTS

Asymmetric direction-alternating optokinetic stimulation is sufficient to elicit set-point adaptation and the resulting negative optokinetic afternystagmus

To understand how differences in visual experience may tune the underlying optokinetic set point, and how such a process would further impact the oculomotor behavior, we recorded eye movements before, during, and after optokinetic stimulation in larval zebrafish five days postfertilization. Figure 1 depicts the experimental setup and the different stimulus paradigms of the current study. Specifically, unidirectional, symmetric direction-alternating (SA), and asymmetric direction-alternating (AA) stimulation were applied (Figure 1C). Figure S1A shows a representative eye-position trace and the corresponding slow-phase velocity (SPV) of zebrafish larvae under unidirectional stimulation—the typical experimental procedure to elicit negative OKAN. During the pre-stimulus dark period, the eyes of the fish spontaneously beat to an eccentric position, followed by centripetal eye drift owing to the leaky velocity-to-position integrator in larval zebrafish (Chen et al., 2014). The beating directions were not biased toward either side. During the 10-min OKN period, the SPV decreased over time, indicating an ongoing set-point adaptation of the retinal slip velocity. During the post-stimulus dark period, there was robust negative OKAN which manifested as eye drifts, with SPV occurring in a direction opposite to the previous OKN. In contrast to the unidirectional stimulation, with symmetric direction-alternating stimulation of +/−10 deg/sec stimulus velocities alternating every 15 s (10/10 SA stimulation, Figure 1Cii) did not lead to an observable OKAN in the majority of the animals (Figure 2A). To examine whether introducing different velocities in the two directions would give rise to negative OKAN, we applied two different asymmetric direction-alternating stimulation paradigms: 10 deg/sec in one direction and −5 deg/sec in the opposite direction (10/5 AA stimulation, Figure 1Ciii), and 20 deg/sec in one direction and −5 deg/sec in the opposite direction (20/5 AA stimulation, Figure 1Civ). After the 10/5 AA stimulation, in most larvae no obvious OKAN was observed (Figure S1B). In contrast, after the 20/5 AA stimulation, most larvae displayed a robust negative OKAN with SPV directing opposite to the faster stimulus velocity (Figure 2B). Collectively, these data reveal that unidirectional stimulation is not necessary. Rather, velocity asymmetry under the AA stimulation is sufficient to elicit negative OKAN.

University Hospital, University of Bern, Switzerland

[13]Lead contact

*Correspondence: tingfenglin.ac@gmail.com (T.-F.L.), melody.yingyu.huang@gmail.com (M.Y.-Y.H.)

https://doi.org/10.1016/j.isci.2022.105335

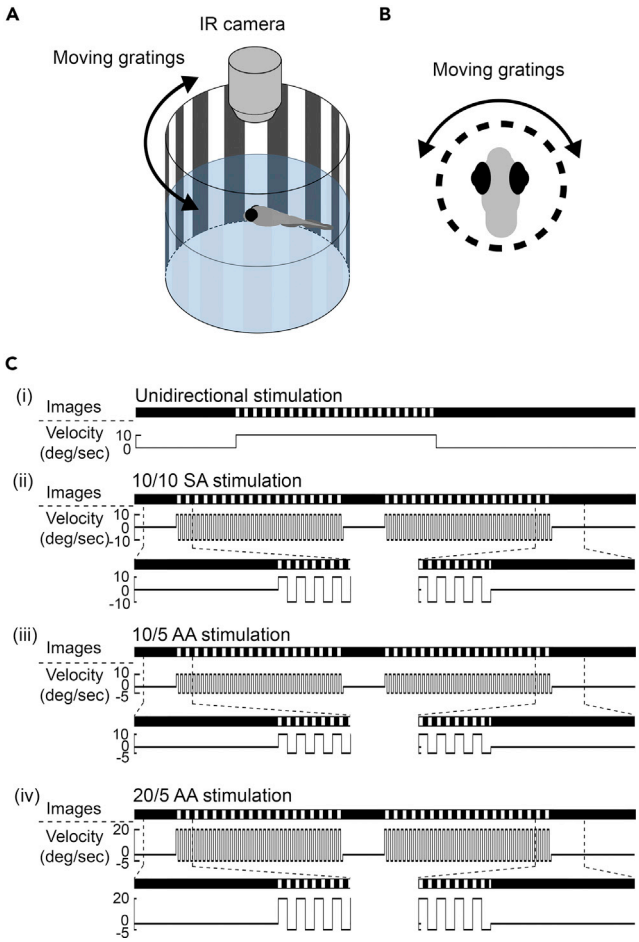

Figure 1. Experimental design to elicit optokinetic set-point adaptation in larval zebrafish

(A and B) Experimental setup of eye recording in larval zebrafish. Individual larval zebrafish were restrained with agarose and placed in the middle of an optokinetic cylinder. Optokinetic nystagmus (OKN) was elicited by moving gratings projected on the cylinder and recorded by an infrared (IR) camera on top of the fish.

(C) From top to bottom, schematic illustrations show optokinetic stimulations with (i) unidirectional +10 deg/sec, (ii) +/−10 deg/sec symmetric alternating (10/10 SA), (iii) +10/−5 deg/sec asymmetric alternating (10/5 AA), and (iv) +20/−5 deg/sec asymmetric alternating (20/5 AA) stimulus velocities. Under all stimulus conditions, a 5-min pre-stimulus dark period and a 10-min post-stimulus dark period were included. Stimulus duration was 10 min for (i) and twice 20 min with a 5-min inter-stimulus dark period for (ii)-(iv).

Asymmetric optokinetic stimulation can lead to set-point adaptation and give rise to the subsequent negative optokinetic afternystagmus

To quantify and compare the oculomotor responses to symmetric and asymmetric stimulation, we computed the population-median SPV under both 10/10 SA and 20/5 AA stimuli. Under 10/10 SA stimulation, the SPV decreased equally in both OKN directions over time, and no negative OKAN developed after the stimulation (Figures 3B-3D). On the contrary, under 20/5 AA stimulation, the SPV only gradually decreased in the direction of the faster stimulus (+20 deg/sec), while remaining mostly unchanged in the other direction (−5 deg/sec). This led to mitigated OKN asymmetry over time despite the sustaining stimulus velocity difference in both directions. Moreover, negative OKAN appeared after the stimulation (Figures 3E–3G). However, such asymmetric SPV adaptation and the subsequent negative OKAN were not obvious in the milder AA stimulation group (10/5 AA, Figure S2). Furthermore, we computed and compared the SPVs of temporal and nasal eye movements to see if the general optokinetic temporal-nasal (T-N) asymmetry (Bonaventure et al., 1983; Braun and Gault, 1969; De'sperati et al., 1994; Gioanni et al., 1981; Hess et al., 1985; Huang and Neuhauss, 2008; Keng and Anastasio, 1997; Klar and Hoffmann, 2002; Mueller and Neuhauss, 2010; Qian et al., 2005; Wallman, 1993; Wallman and Velez, 1985) was preserved

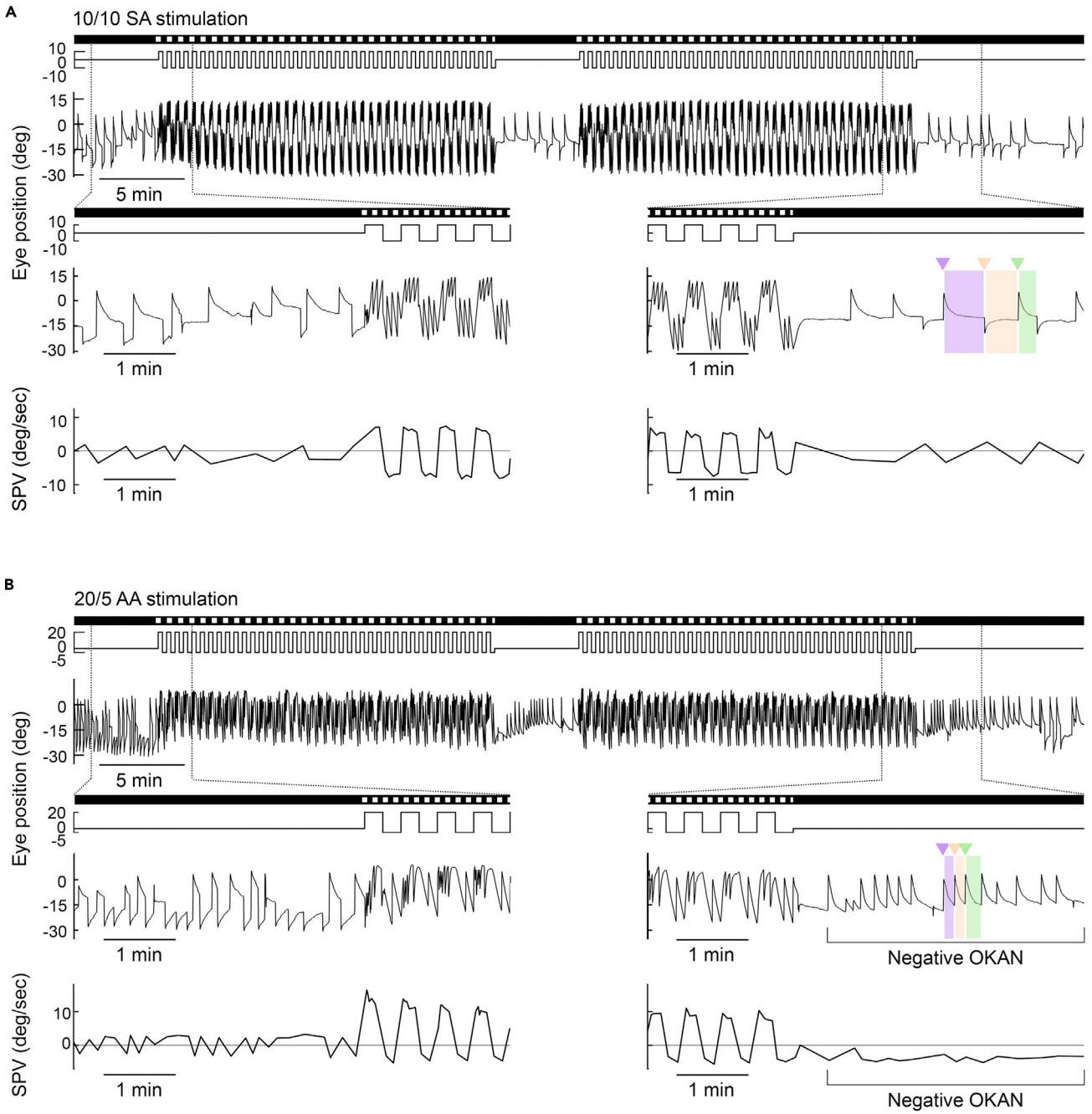

Figure 2. Negative OKAN can be elicited by asymmetric optokinetic stimulation

(A and B) Typical eye-position traces with corresponding slow-phase velocities (SPVs) of zebrafish larvae under 10/10 symmetric alternating (SA) (A), and 20/5 asymmetric alternating (AA) (B) stimulations. The SPV was estimated as the median velocity in the first second of each slow phase (shaded area) after discarding the quick-phase eye movement (triangle). The stimulus image pattern (darkness or gratings) and the stimulus velocity are shown on the top as horizontal bars and lines, respectively. At the bottom, the magnified traces are shown to better demonstrate the transition phases from pre-stimulatory darkness to optokinetic nystagmus (OKN) and from OKN to post-stimulatory darkness. Positive values represent movements to the left (counterclockwise), and negative values represent movements to the right (clockwise).

under sustained AA stimulation. Interestingly, the T-N asymmetry was only recorded under 10/10 SA and 10/5 AA stimulation and was no longer observable under 20/5 AA stimulation (Figure S3), suggesting that significant stimulus velocity differences between left and right directions may prevail over the inherent T-N asymmetry.

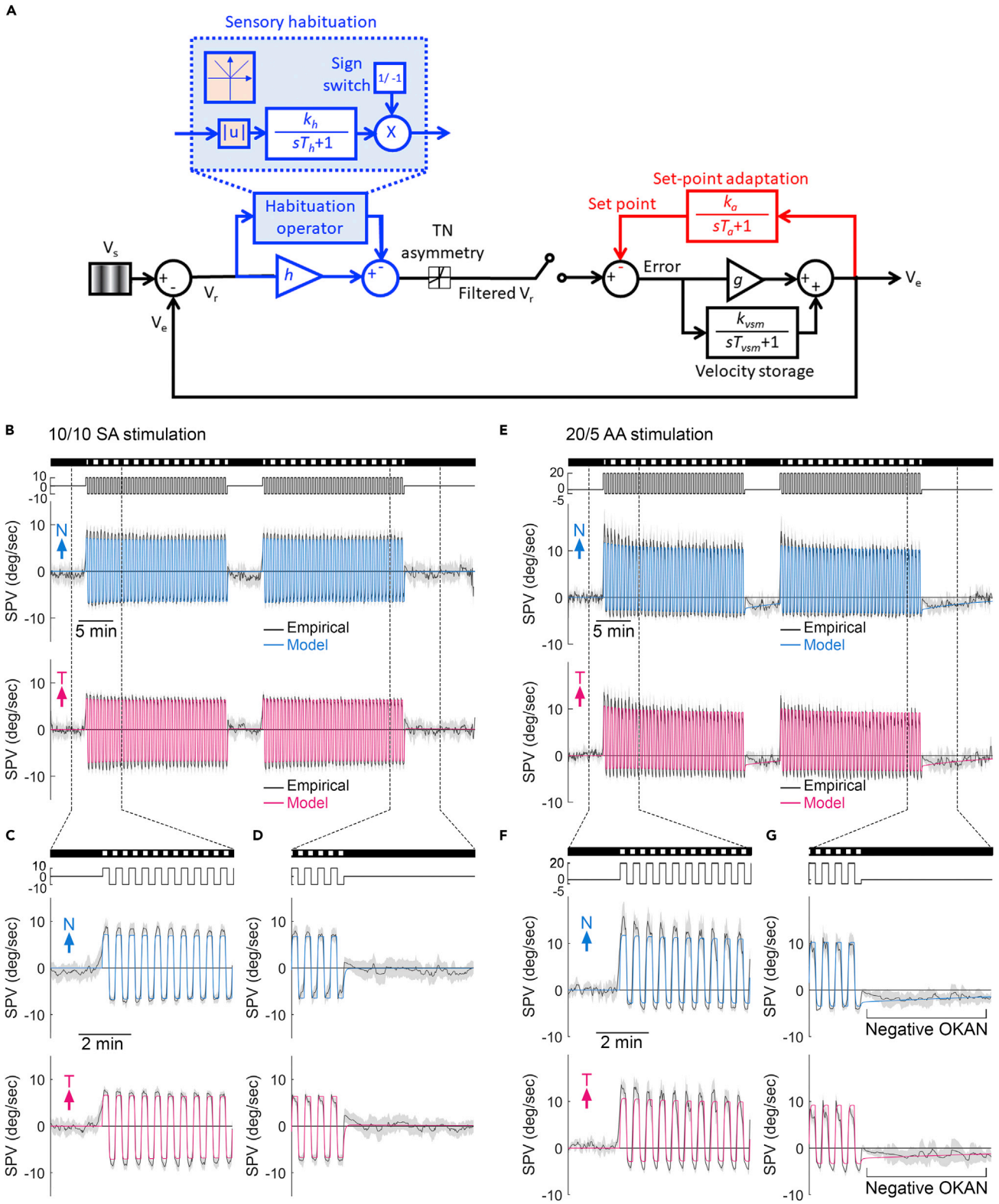

Figure 3. Optokinetic set-point adaptation model predicts the recorded SPV in larval zebrafish

(A) The mathematical model of set-point adaptation. Retinal slip velocity (V_r) is the difference between the stimulus velocity (V_s) and the eye velocity (V_e). During habituation, V_r is rectified and filtered with a time constant of T_h and gain of k_h (blue shaded area), and then scaled with h, to give a filtered V_r. In the

Figure 3. *Continued*

sensory habituation operator, |u|, which produces the absolute value of the input (orange shaded area), together with a sign switch of output lead to a continuous habituating effect regardless of stimulus direction. The filtered V_r passes through a nonlinear gain (T-N gain) that captures the T-N asymmetry. The error between the filtered V_r and the set point is scaled by oculomotor gain (g) and added to the velocity storage mechanism (VSM) to control V_e. VSM contains a leaky integrator with a time constant of T_{vsm} and a gain of k_{vsm} that contributes to the eye velocity. V_e is then integrated with a time constant of T_a and a gain of k_a to adjust the set point.

(B–G) The model predicted population-median SPV (colored lines) superimposed on the median ± median absolute deviation (black line with gray shadow) of empirical SPVs during 10/10 symmetric alternating stimulations (SA, n = 29) (B–D) and 20/5 asymmetric alternating stimulations (AA, n = 18) (E–G). Considering the starting direction of alternating stimulation was randomized, we aligned the first stimulus direction as positive instead of left or right. Therefore, the plots show one eye started with a nasalward movement (blue trace) and another eye started with a temporalward movement (red trace). The stimulus image pattern (darkness or gratings) and the stimulus velocity are shown on the top as horizontal bars and lines, respectively.

Mathematical model of negative optokinetic afternystagmus

To gain an understanding of the nature of the mechanisms that enable negative OKAN under AA but not SA stimulation, we built a mathematical model that incorporated both sensory habituation and set-point adaptation (Lin et al., 2019) but was adapted to account for bidirectional stimulation (Figure 3A, see STAR methods). Best-fit parameter values were obtained by using one-half of the behavioral dataset for a given stimulation condition, and quantifying goodness-of-fit using the other half of the dataset (see STAR methods).

Overall, our model successfully reproduced experimentally observed eye movements under direction-alternating stimulation (Figures 3 and S2). Specifically, Figure 3 shows the model-predicted SPV in comparison with the empirical data under both 10/10 SA (Figures 3B–3D) and 20/5 AA (Figures 3E–3G) stimulation. Generally, the set-point adaptation operator of the model is counteractively charged with opposite signs under the alternating cycles of the stimulus directions. Through SA stimulation, the inputs with opposite signs cancel each other out, resulting in an unchanged set point value of around 0 deg/sec. In comparison, under AA stimulus conditions, the adaptation integrator is charged more in the faster-stimulus direction than the other. As a result, a set point is built over time. Conceptually, the changed set point alone is expected to reduce the SPV in the direction of the faster stimulus but increase it with an equal value in the opposite direction. However, with the incorporation of sensory habituation, the model predicts a relatively stable SPV in the slower-stimulus direction yet an SPV with a significant velocity reduction in the faster-stimulus direction (Figures 3E–3G). Furthermore, during the post-stimulation period after the 20/5 AA stimulus, the non-zero set point leads to negative OKAN (Figure 3G). Similarly, our model also predicts SPV analogous to the experimental data under a 10/5 AA stimulus (Figure S2). Notably, although our model also predicts negative OKAN after 10/5 AA stimulation (albeit weaker than the 20/5 AA condition), it was not obvious in the experimental data.

Individual larvae displayed behavioral asymmetries under symmetric optokinetic stimulation

Based on the population SPV median, only the asymmetric stimulation would elicit set-point adaptation and the resulting negative OKAN (Figure 3). Surprisingly, however, eye-position traces revealed that some individual larvae did develop negative OKAN under symmetric stimulation. Figure 4A depicts a representative trace of a larva that displayed robust negative OKAN following 10/10 SA stimulation. We wondered whether this indicated that the preceding SPV was biased toward one direction. To overcome the challenge of spotting minor behavioral asymmetries in the left-right directions on top of the robust T-N asymmetry (Bonaventure et al., 1983; Braun and Gault, 1969; De'sperati et al., 1994; Gioanni et al., 1981; Hess et al., 1985; Huang and Neuhauss, 2008; Keng and Anastasio, 1997; Klar and Hoffmann, 2002; Mueller and Neuhauss, 2010; Qian et al., 2005; Wallman, 1993; Wallman and Velez, 1985), we computed the SPV median of the population (n = 29), applied it as the standard response curve, then compared that with single larva's behavior (Figures 4B–4D). Indeed, the analyzed results confirmed that, compared to the population median, the representative larva displays a faster SPV in the positive direction but a similar SPV in the other direction during early OKN (Figure 4C), followed by negative OKAN in the negative direction (Figure 4D). To better visualize the SPV difference, we subtracted the population median from the individual's SPV, denoted as ΔSPV (Figures 4E–4G). The ΔSPV of the representative individual is biased in a positive direction during the early OKN (Figure 4F); moreover, throughout the stimulation, the asymmetry becomes slightly mitigated, as shown during the late OKN (Figure 4G).

To quantify the asymmetric responses and the resulting adaptation under symmetric stimulation across individuals, we computed average ΔSPVs for each subject within a time window of 4 min before, at the

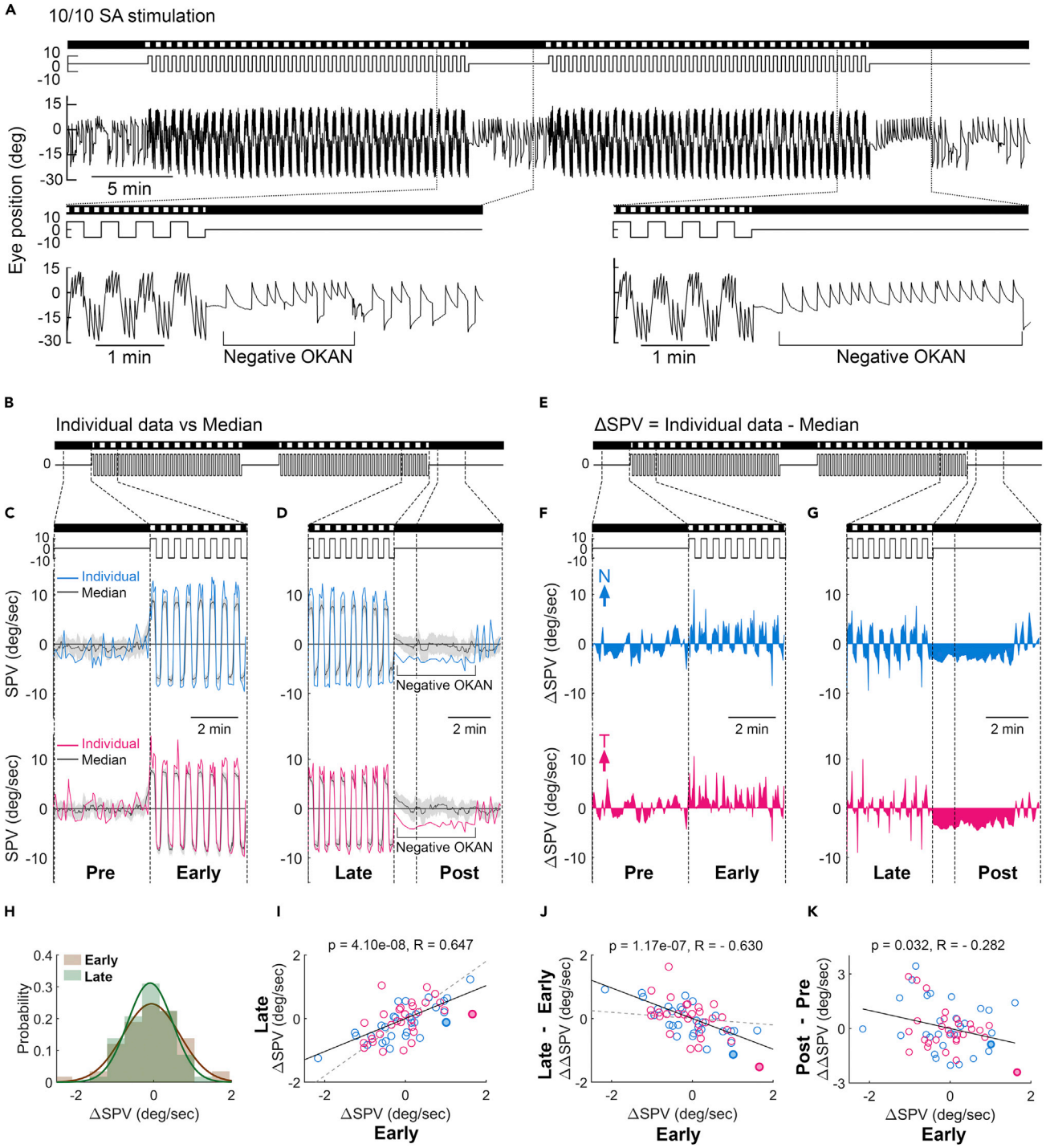

Figure 4. Zebrafish larvae display different levels of asymmetric OKN under the symmetric stimulus

(A) A typical eye-position trace of a single larva with an asymmetric optokinetic nystagmus (OKN) under 10/10 symmetric alternating (SA) stimulation and the following negative optokinetic afternystagmus (OKAN). The bottom plots show magnifications to demonstrate the transition phases from OKN to inter- and post-stimulatory periods, respectively.

(B and E) The stimulus image pattern and the stimulus velocity are shown as horizontal bars and lines, respectively.

(C and D) The slow-phase velocity (SPV) of (A, color line) is compared to the median ± median absolute deviation of 29 subjects (black line with gray shadow).

(F and G) The difference in SPVs between the individual larva (color line in C and D) and the population median (black line in C and D). Dashed lines extend from (E) to (F and G) illustrate the time windows for further analyses in (H–K).

Figure 4. *Continued*

(H) The ΔSPV probability distribution of 29 fish during the early and late periods. Two lines demonstrate the fit of distributions with Gaussian function.
(I) The late ΔSPV plotted over the early ΔSPV. The slope of the linear regression line (solid line) is significantly smaller than 1 (p = 1.79e-08; interactive analysis of covariance) and the slope of the dashed line (temporally shuffled data; p = 4.21e-06; interactive analysis of covariance).
(J) The changes in ΔSPV across stimulus phases (late ΔSPV – early ΔSPV, ΔΔSPV) plotted over the early ΔSPV. The slope of linear regression line (solid line) is significantly lower than the slope of the dashed line (temporally shuffled data; p = 4.21e-06; interactive analysis of covariance).
(K) The changes of the eye movements in the dark before and after OKN (post-ΔSPV – pre-ΔSPV, ΔΔSPV) plotted over the early ΔSPV. Filled circles represent the data of the animal shown in (A). Black solid lines demonstrate the linear regression fit of recorded data. Considering the starting direction of alternating stimulation was randomized, we aligned the first stimulus direction as positive instead of left or right. Therefore, the plots show one eye started with a nasalward movement (blue trace) and another eye started with a temporalward movement (red trace). p, p values; Pearson correlation. R, correlation coefficients; Pearson correlation.

beginning of, at the end of, and after the OKN, depicted as pre, early, late and post, respectively (Figures 4E–4G). We skipped the first minute post-stimulus to avoid the influence of the velocity storage (Lin et al., 2019). Probability distribution plots revealed that data of both early and late OKN display normal distributions centered at around 0 deg/sec (Figure 4H). Notably, compared to the early OKN period, the bell curve of ΔSPV in the late OKN generates a taller and narrower shape, which corresponds to the mitigated behavioral asymmetry over prolonged stimulation and thus less ΔSPV data distributed at two tails. Next, we plotted the late ΔSPV over the early ΔSPV. A Pearson correlation test revealed a significant positive correlation, and the slope of regression line is significantly smaller than 1 (Figure 4I), consistent with the reduced variance of the late ΔSPV distribution (Figure 4H). In other words, fewer fish showed behavioral asymmetry after a prolonged period of symmetric stimulation. To avoid data misinterpretation owing to regression toward the mean (Furrow, 2019), we additionally computed and compared our data with the null expectation derived from the temporally shuffled data (Figures 4I and S4; see STAR methods). We then computed the changes in ΔSPV across stimulus phases (late ΔSPV – early ΔSPV, ΔΔSPV) and plotted them over the early ΔSPV (Figure 4J). Our data revealed a negative correlation with a significantly smaller regression-line slope compared to the regression-line slope of the shuffled data, implying that greater inherent behavioral asymmetries (i.e., early ΔSPV) would lead to a higher degree of the optokinetic set-point adaptation. The gradual reduction of the behavioral asymmetry can be further seen in Figure S4. Finally, we also found a significant negative correlation between changes in eye movements in the dark before and after OKN (post-ΔSPV – pre-ΔSPV, ΔΔSPV) and the early ΔSPV (Figure 4K), which further suggests the dependency of negative OKAN on the inherent OKN asymmetry.

Degrees of innate bias are accountable for different behavioral asymmetries and inter-individual variations

Based on the empirical data, we hypothesize that under symmetric stimulation, individual larvae that underwent set-point adaptation and developed the resulting negative OKAN may embrace an innate directional bias within the optokinetic system. To validate this conceptual model, we introduced a constant value for "bias" (Figure 5A). Indeed, under symmetric stimulation, varying this value can predict either no asymmetry (Figures 5B–5D) or robust asymmetry (Figures 5E–5G) in SPV in both directions, with the latter also predicting the resulting negative OKAN.

Next, we optimized the parameter fitting for each larva to estimate the innate bias based on its individual empirical data. The distribution of the estimated innate bias is computed and depicted in Figure 5H. As the distribution is roughly symmetric and centers at 0 deg/sec with a few outliers biased in either direction, empirically the population median SPV does not show asymmetric OKN or negative OKAN. Furthermore, not only does the innate bias predict the ΔSPV (Figures 5I and 5J; the same ΔSPV data are shown in Figure 4I), but it reveals a higher correlation coefficient with the early ΔSPV (Figure 5I) than with the late ΔSPV (Figure 5J), suggesting that the innate bias-caused ocular motor asymmetry can be compensated by set-point adaptation. The bias also predicts the change in eye movements in the dark (post-ΔSPV – pre-ΔSPV, ΔΔSPV; Figure 5K), suggesting that negative OKAN is dependent on innate bias. In conclusion, adjusting the innate bias in the model will predict the magnitude of behavioral asymmetry and the resulting set-point adaptation.

Finally, we applied the estimated biases to simulate ΔSPV (Figures 6A–6F) in all subjects. Overall, the model simulation predicts all critical features revealed by the empirical data (Figure 6, compared to Figure 4). Specifically, the variance of the ΔSPV distribution is reduced throughout the stimulation (Figures 6G–6I and S5). We also found a significant negative correlation between the change in eye movements in the

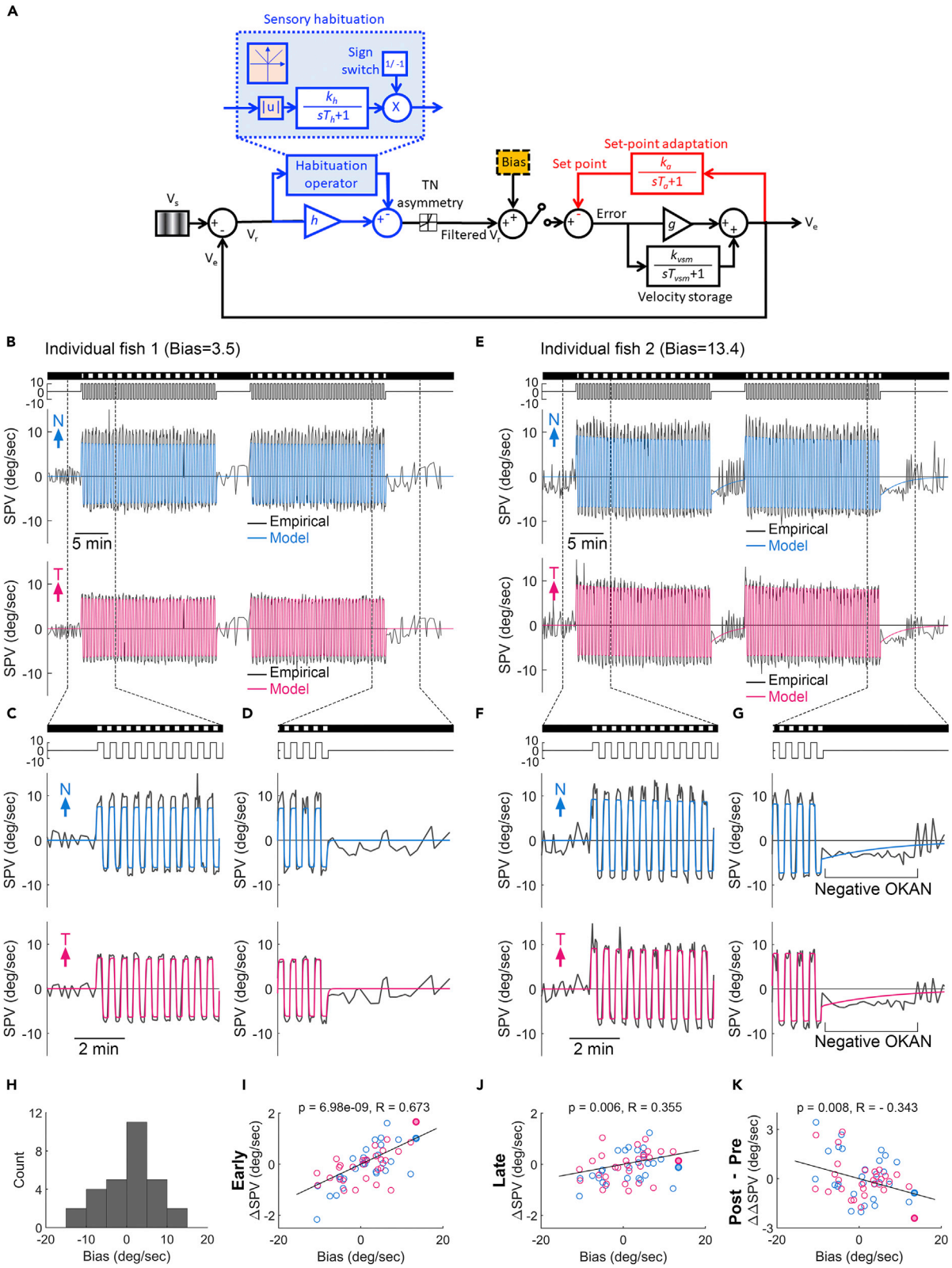
A
Sensory habituation
Sign switch
1/ -1
|u|
$\frac{k_h}{sT_h+1}$
X
Habituation operator
h
TN asymmetry
Filtered V_r
Bias
Set-point adaptation
Set point
$\frac{k_a}{sT_a+1}$
Error
g
$\frac{k_{vsm}}{sT_{vsm}+1}$
Velocity storage
V_s
V_r
V_e
B
Individual fish 1 (Bias=3.5)
E
Individual fish 2 (Bias=13.4)
SPV (deg/sec)
N
T
5 min
Empirical
Model
C
D
F
G
2 min
Negative OKAN
H
Count
Bias (deg/sec)
I
p = 6.98e-09, R = 0.673
Early
ΔSPV (deg/sec)
J
p = 0.006, R = 0.355
Late
K
p = 0.008, R = - 0.343
Post - Pre
ΔΔSPV (deg/sec)

Figure 5. An innate bias in the optokinetic system accounts for the asymmetric OKN and the corresponding set-point adaptation under the symmetric stimulus

(A) A modified mathematical model to explain the asymmetric optokinetic nystagmus (OKN) gain under symmetric stimulation and the following optokinetic afternystagmus (OKAN). The design is based on the proposed model shown in Figure 3A; however, a constant innate bias (yellow box) is introduced to the optokinetic system.

(B–G) The model predicted slow-phase velocity (SPV, colored lines) superimposed on the empirical SPVs of individual subjects (black lines) with symmetric (B–D) and asymmetric (E–G) eye movements.

(E) is the same data shown in Figure 4A. Considering the starting direction of alternating stimulation was randomized, we aligned the first stimulus direction as positive instead of left or right. Therefore, the plots show one eye started with a nasalward movement (blue trace) and another eye started with a temporalward movement (red trace). The stimulus image pattern (darkness or gratings) and the stimulus velocity are shown on the top as horizontal bars and lines, respectively.

(H) The fish counts of the estimated bias (total fish number = 29).

(I–K) The early ΔSPV (I), late ΔSPV (J), and the changes of the eye movements in darkness before and after OKN (post-ΔSPV – pre-ΔSPV, ΔΔSPV) (K) plotted over the estimated bias. V_s, stimulus velocity. V_e, the eye velocity. V_r, the retinal slip velocity. V_e, eye velocity. T_h, habituation time constant. k_h, habituation gain. |u|, absolute operator. *g*, oculomotor gain. T_{vsm}, velocity storage time constant. k_{vsm}, velocity storage gain. T_a, set-point adaptation time constant. k_a, set-point adaptation gain. p, p-values; Pearson correlation. R, correlation coefficients; Pearson correlation.

dark (post-ΔSPV – pre-ΔSPV, ΔΔSPV) and the early ΔSPV (Figure 6J). Altogether, the model is generalizable across individuals, and the innate bias spectrum is accountable for the inter-individual variation.

Finally, in addition to the proposed model, we further tested an alternative model by introducing an innate bias at the motor level (Figure S6). However, the innate bias at the motor level drives a behavioral asymmetry prior to the optokinetic stimulus (Figure S6F) which fails to predict our empirical observation. Also, this alternative model does not reproduce the compensation of behavioral asymmetry throughout the symmetric stimulation (Figures S6H–S6J).

DISCUSSION

In vertebrates, a stable oculomotor system relies on precise sensorimotor control and coordination, which largely involves both the visual and vestibular systems. The optokinetic system plays an essential role in stabilizing the retina with respect to the visual surroundings. Any disturbance or malfunction in the system may cause oculomotor disequilibrium and interfere with accurate sensorimotor transformation. In the current study, we describe two types of directional eye movement bias in the optokinetic system: the typical T-N asymmetry existing in most lateral-eyed animals (Bonaventure et al., 1983; Braun and Gault, 1969; De'sperati et al., 1994; Gioanni et al., 1981; Hess et al., 1985; Huang and Neuhauss, 2008; Keng and Anastasio, 1997; Klar and Hoffmann, 2002; Mueller and Neuhauss, 2010; Qian et al., 2005; Wallman, 1993; Wallman and Velez, 1985) and a left-right asymmetry that can readily be triggered by an asymmetric stimulus in a laboratory setting. On top of that, we noted an innate bias in the optokinetic system that can equally cause left-right asymmetry in some animals. The aim of this study was to scrutinize how the optokinetic system applies set-point adaptation to adjust for oculomotor asymmetries.

Set-point adaptation results from the temporal integration of visual experience

Compared to negative OKAN, positive OKAN refers to another aftereffect in which eyes move in the same direction as the preceding OKN. This is attributed to the velocity storage mechanism (VSM), which helps estimate head motion (Laurens and Angelaki, 2011). VSM-associated positive OKAN is relatively short-lasting and can be evoked by just 2 s of optokinetic stimulation (Buttner et al., 1976), which then lasts up to 1-2 min (Brandt et al., 1974; Cohen et al., 1981; Demer and Robinson, 1983; Waespe and Henn, 1977; Yokota et al., 1992). Furthermore, the stored velocity is sensitive to and can be rapidly discharged by cerebellar uvula in response to variation in visual (Waespe et al., 1978, 1985) and vestibular (Waespe et al., 1985) sensory inputs. In contrast to VSM, optokinetic set-point adaptation has recently been proposed as a novel underlying mechanism to compensate for persisting asymmetric sensory input from the periphery and can manifest as another distinct longer-lasting oculomotor aftereffect—the negative OKAN (Lin et al., 2019). Except for a few pathological situations, however, it is not common for animals to consistently turn their bodies so that rotation is always perceived in the same direction. Intuitively, the brain should be capable of rendering set-point adjustment under dynamic visual conditions and thus extract and estimate the net sensory asymmetry over an extended period of time. Our results indeed show that unidirectional stimulation is not necessary, but direction-alternating stimulation is sufficient to generate negative OKAN as the result of a temporally integrated set-point adaptation. This finding demonstrates very distinct

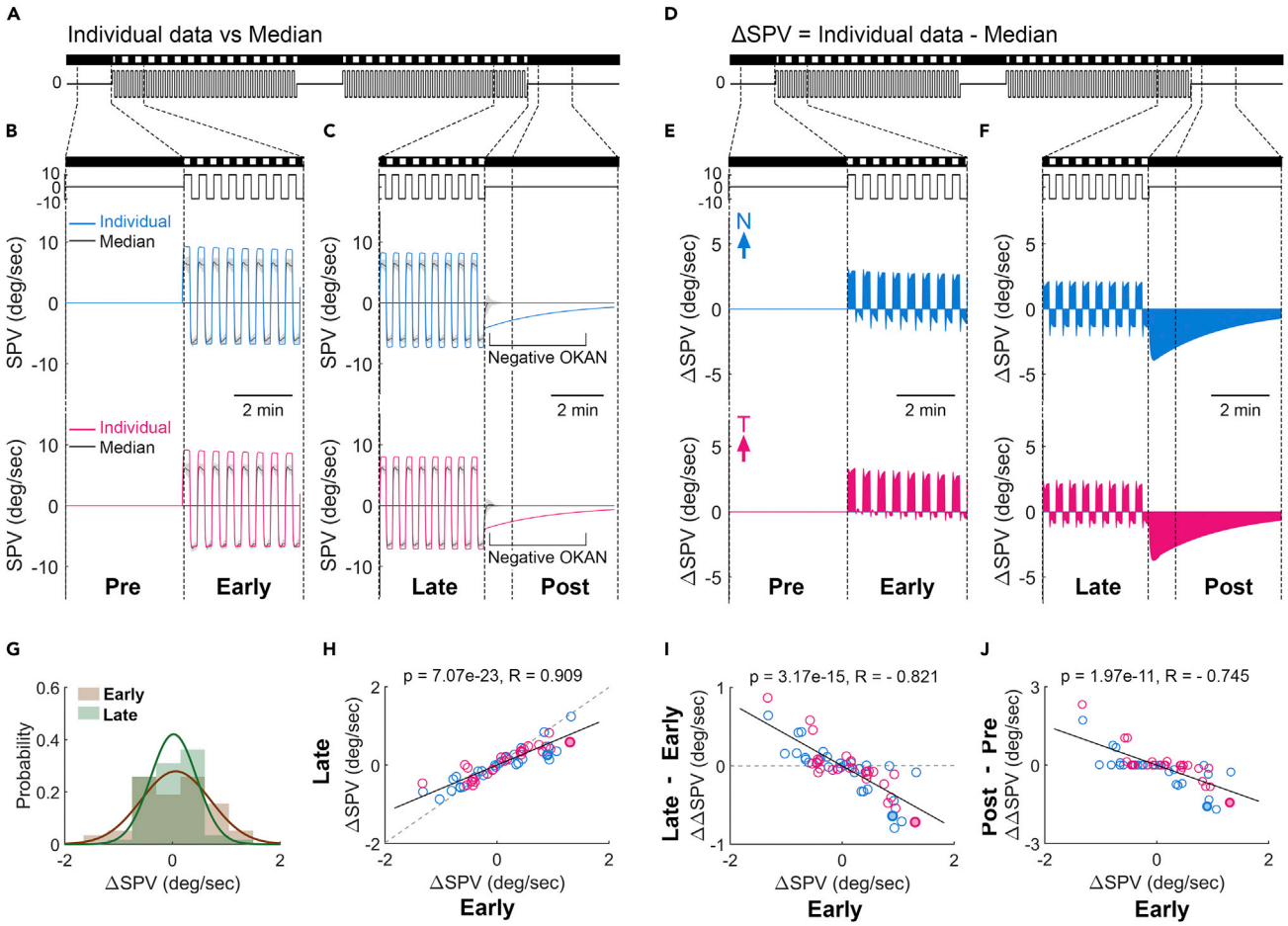

Figure 6. The model is generalizable across individuals

(A and D) The stimulus image pattern and the stimulus velocity are shown as horizontal bars and lines, respectively.

(B and C) The simulated slow-phase velocity (SPV) of Figure 4A (color line) is compared to the median ± median absolute deviation of simulations from all 29 subjects (black line with gray shadow).

(E and F) The difference of SPVs between the individual simulation (color line in B and C) and the population median (black line in B and C). Dashed lines extend from (D) to (E and F) illustrate the time windows for further analyses in (G–J).

(G) The ΔSPV probability distribution of 29 fish during the early and late periods. Two lines demonstrate the fit of distributions with Gaussian function.

(H) The late ΔSPV plotted over the early ΔSPV. The slope of linear regression line (solid line) is significantly smaller than 1 ($p = 5.58e-19$; interactive analysis of covariance) and the slope of the dashed line (temporally shuffled data; $p = 1.94e-18$; interactive analysis of covariance).

(I) The changes in ΔSPV across stimulus phases (late ΔSPV – early ΔSPV, ΔΔSPV) plotted over the early ΔSPV. The slope of linear regression line (solid line) is significantly lower than the dashed line (temporally shuffled data; $p = 1.94e-18$; interactive analysis of covariance).

(J) The changes of the eye movements in the dark before and after optokinetic nystagmus (post-ΔSPV – pre-ΔSPV, ΔΔSPV) plotted over the early ΔSPV. Filled circles represent the data of the animal shown in (A–F).

(H and I) Black solid lines demonstrate the linear regression fit of simulated data. Considering the starting direction of alternating stimulation was randomized, we aligned the first stimulus direction as positive instead of left or right. Therefore, the plots show one eye started with a nasalward movement (blue trace) and another eye started with a temporalward movement (red trace). p, p values; Pearson correlation. R, correlation coefficients; Pearson correlation.

characteristics of set-point adaptation and the resulting negative OKAN compared to the VSM and the resulting positive OKAN (Waespe et al., 1978, 1985).

An innate bias in the oculomotor system can lead to optokinetic nystagmus asymmetry and negative optokinetic afternystagmus

The exploratory behavior of zebrafish reveals overall symmetric distribution between the left and right turning angles (Dunn et al., 2016; Goc et al., 2021). Since the general visual experience in real life should

be directionally symmetric, we asked ourselves what the physiological necessity of the underlying set-point adaptation is. We observed that not all animals developed a perfectly symmetric optokinetic system. On the contrary, some animals displayed OKN asymmetry under symmetric stimulation, followed by negative OKAN (Figure 4). It is worth noting that, analogous to the asymmetric OKN and the subsequent negative OKAN in healthy animals, patients with latent nystagmus (MLN) and infantile nystagmus syndrome (INS) (Shawkat et al., 2001) and as well the zebrafish INS model *belladonna* strain (Huang et al., 2006; Huber-Reggi et al., 2012) exhibit direction-asymmetric spontaneous nystagmus in light followed by negative OKAN in darkness (Shawkat et al., 2001 for patients, and unpublished data for zebrafish).

To conceptualize factors that affect the oculomotor behavioral asymmetry, we introduce a constant "innate" directional bias to the mathematical model, incorporating sensory habituation and set-point adaptation (Figure 5A). Indeed, the model predicts behavioral asymmetry of OKN (Figures 5E–5G) which varies across animals (Figure 6G), in line with the varying innate biases within the population (Figure 5H). Furthermore, this model also successfully predicts the mitigated OKN asymmetry over the stimulus period and the post-stimulus negative OKAN (Figure 6), phenocopying the empirical data (Figure 4). Accordingly, we argue that an innate bias can cause an asymmetric OKN which is attenuated by set-point adaptation.

Since all animals used for the present study were wild-type and carried no artificially induced factor that might cause behavioral asymmetry, we wondered why and in what situation an innate bias might evolve in animals. In the young brain, coarse neural wiring has to be in place under molecular guidance, but experience-dependent fine-tuning remains in effect and critical (Cline, 2003). Prior to the fine-tuning, it's conceivable that inherent structural and functional asymmetry could just arise stochastically by nature. In fact, an unwanted developmental asymmetry during the early developmental stage is not uncommon. For example, the initial somite development in zebrafish embryos often shows asymmetry in length and position between left and right, and later at the fine-tuning stage, this asymmetry can be adjusted by the molecular signaling according to the surface tension (Naganathan et al., 2022). The set-point adaptation may play an analogous role in fine-tuning the optokinetic system to continuously seek a state of equilibrium through the symmetric visual experience. We might also expect an innate bias deriving from unilateral/asymmetric physical conditions associated with injuries or diseases.

Comparable cases have also been reported in the vestibular system. To estimate head rotation on the horizontal plane, signals from both sides of the vestibular end organs are constantly compared. The imbalance of rotational signals from the two sides owing to a unilateral vestibular loss can lead to a vestibular behavioral asymmetry—the vestibular nystagmus (Fetter and Zee, 1988). The subsequent recovery process has been described as a set-point adaptation mechanism (Zee et al., 2017). In the current study, a similar mathematical framework of the vestibular set-point adaptation (Jareonsettasin et al., 2016; Leigh et al., 1981; Zee et al., 2017) has been constructed to simulate the adaptation process under optokinetic asymmetry, and the results validate the applicability of the model to explain the empirical phenomena.

Multiple underlying mechanisms of set-point adaptation in the oculomotor system

Besides the behavioral aspects of the optokinetic set-point adaptation, there have been several valuable research works using molecular markers and/or neural activity recordings to investigate its underlying mechanisms. The results have suggested multiple processing stages and pinpointed the involved brain areas. A recent study identified the pretectum as crucial for initiating negative OKAN in zebrafish larvae (Wu et al., 2020). The initial behavior-compensating mechanism may be relatively short and temporary; however, the underlying ongoing molecular events may further shape the anatomical and functional neural circuits to maintain equilibrium. Various biochemical experiments have demonstrated that prolonged unidirectional optokinetic stimulation leads to changes in the molecular expression profile that are known to play roles in the neural plasticity of floccular Purkinje cells (Barmack and Qian, 2002; Barmack et al., 2010, 2014; Qian et al., 2012). Thus, it is conceivable that the corresponding molecular signaling cascades may underlie or consolidate the dynamic calibration process during oculomotor controls.

The link between negative OKAN and the vestibular nucleus was identified in the past (Waespe and Henn, 1977). Relevant studies in the vestibular nucleus may potentially shed light on the underlying mechanisms of the optokinetic set-point adaptation. In laboratory rodents, unilateral labyrinthectomy has been introduced to model the long-term vestibular imbalance and the subsequent functional restoration (Darlington and Smith, 2000). Owing to the synaptic (Johnston et al., 2001; Lim et al., 2010; Vibert et al., 2000) and

intrinsic (Nelson et al., 2017) plasticity of the vestibular nucleus, animals recovered from the surgery-induced behavioral imbalance. However, in mice that underwent unilateral labyrinthectomy, the ipsilesional vestibular nucleus showed increased excitability within 24 h of the injury but returned to its normal firing state while the behavioral restoration remained (Nelson et al., 2017). This further suggests that, in addition to the vestibular nucleus plasticity, multiple mechanisms were involved in the compensating tasks. To obtain a comprehensive understanding of the dynamic mechanisms underlying set-point adaptation in different sensory systems, further mechanistic studies—including a screening of larger-scale functional brain networks—will be indispensable.

Limitations of the study

In the current study, we reported a left-right asymmetry of optokinetic gain that naturally occurs at the early developmental stage of wild-type larval zebrafish and demonstrated a fine-tuning sensory adaptation mechanism in the optokinetic system that helps to compensate for the naturally occurring neurobehavioral disequilibrium. However, the alternating duration of stimulus in nature is dynamic and averaged at around 6 s (Dunn et al., 2016), which was not perfectly copied by our optokinetic paradigm. Also, a relatively strong visual stimulus (i.e., high contrast and stimulus velocity) was given within a relatively short (i.e., 1 h) recording period. Experiments with milder stimuli but longer recording time or with repeated exposures could simulate the natural conditions more closely and might generate a longer-lasting adaptation. Although the set-point adaptation functioning as an internal calibration mechanism for oculomotor disequilibrium is evident in zebrafish following our current experimental procedure, to understand its role in neural development, further investigation on cross-age comparison of innate bias in zebrafish that are raised in a relatively natural environment will be necessary.

STAR★METHODS

Detailed methods are provided in the online version of this paper and include the following:

- KEY RESOURCES TABLE
- RESOURCE AVAILABILITY
  - Lead contact
  - Materials availability
  - Data and code availability
- EXPERIMENTAL MODEL AND SUBJECT DETAILS
  - Larval zebrafish
- METHOD DETAILS
  - Visual stimulation
  - Stimulus procedure
  - Eye movement recording and analysis
  - Model
  - Parameter estimation
- QUANTIFICATION AND STATISTICAL ANALYSIS
  - Statistical analysis
  - Randomization test

SUPPLEMENTAL INFORMATION

Supplemental information can be found online at https://doi.org/10.1016/j.isci.2022.105335.

ACKNOWLEDGMENTS

The authors thank Jeannie Wurz for proofreading and editing the article; Jean-Marc Fritschy, Frank Stüber, and Markus Lüdi for providing the resources and support for carrying out this study; Fausto Romano, Dominik Straumann, Marco Penner, Christopher Bockisch, and Urs Scheifele for the technical support and pilot discussions. This work was supported by the Oxford McGill ZNZ Partnership in the Neurosciences Pilot Project Funding (KEC, MJC, and MYH), the National Institutes of Health (KEC, UF1NS111695, R01DC018304, RDC002390, and R01DC018061), the Canadian Institutes of Health Research (MJC), the Research Grant for the Faculty of Medicine, UZH (MYH), the Dr. Dabbous Foundation (T-FL and MYH), the Betty and David Koetser Foundation for Brain Research (T-FL and MYH), the EMDO Stiftung Zürich

(MYH, Gesuch Nr. 942), and an institutional grant from the Department of Anesthesiology and Pain Medicine, Inselspital, Bern (MYH, Gesuch Nr. HEYF-1-22).

AUTHOR CONTRIBUTIONS

T-FL and MYH designed the research, T-FL and MM performed experiments, T-FL, MM, KEC, MJC and MYH performed analyses, and T-FL, MM, and MYH wrote the article. All authors reviewed the article.

DECLARATION OF INTERESTS

The authors declare no competing interests.

Received: June 9, 2022
Revised: September 6, 2022
Accepted: October 10, 2022
Published: November 18, 2022

REFERENCES

Arrenberg, A.B. (2016). Fiber optic-based photostimulation of larval zebrafish. Methods Mol. Biol. *1451*, 343–354. https://doi.org/10.1007/978-1-4939-3771-4_24.

Barmack, N.H., and Nelson, B.J. (1987). Influence of long-term optokinetic stimulation on eye movements of the rabbit. Brain Res. *437*, 111–120. https://doi.org/10.1016/0006-8993(87)91532-0.

Barmack, N.H., and Qian, Z. (2002). Activity-dependent expression of calbindin in rabbit floccular Purkinje cells modulated by optokinetic stimulation. Neuroscience *113*, 235–250. https://doi.org/10.1016/s0306-4522(02)00008-8.

Barmack, N.H., Qian, Z., and Yakhnitsa, V. (2010). Climbing fibers induce microRNA transcription in cerebellar Purkinje cells. Neuroscience *171*, 655–665. https://doi.org/10.1016/j.neuroscience.2010.09.039.

Barmack, N.H., Qian, Z., and Yakhnitsa, V. (2014). Long-term climbing fibre activity induces transcription of microRNAs in cerebellar Purkinje cells. Philos. Trans. R. Soc. Lond. B Biol. Sci. *369*, 20130508. https://doi.org/10.1098/rstb.2013.0508.

Beck, J.C., Gilland, E., Baker, R., and Tank, D.W. (2004). Instrumentation for measuring oculomotor performance and plasticity in larval organisms. Methods Cell Biol. *76*, 385–413. https://doi.org/10.1016/s0091-679x(04)76017-3.

Bever, M.M., and Fekete, D.M. (2002). Atlas of the developing inner ear in zebrafish. Dev. Dynam. *223*, 536–543. https://doi.org/10.1002/dvdy.10062.

Bollmann, J.H. (2019). The zebrafish visual system: from circuits to behavior. Annu. Rev. Vis. Sci. *5*, 269–293. https://doi.org/10.1146/annurev-vision-091718-014723.

Bonaventure, N., Wioland, N., and Bigenwald, J. (1983). Involvement of GABAergic mechanisms in the optokinetic nystagmus of the frog. Exp. Brain Res. *50*, 433–441. https://doi.org/10.1007/BF00239210.

Brandt, T., Dichgans, J., and Büchle, W. (1974). Motion habituation: inverted self-motion perception and optokinetic after-nystagmus. Exp. Brain Res. *21*, 337–352. https://doi.org/10.1007/BF00237897.

Braun, J.J., and Gault, F.P. (1969). Monocular and binocular control of horizontal optokinetic nystagmus in cats and rabbits. J. Comp. Physiol. Psychol. *69*, 12–16. https://doi.org/10.1037/h0027887.

Bures, J., and Neverov, V.P. (1979). Reversed postoptokinetic nystagmus: a model of plasticity in the vestibuloocular system. Acta Neurobiol. Exp. *39*, 477–490.

Büttner, U., Waespe, W., and Henn, V. (1976). Duration and direction of optokinetic after-nystagmus as a function of stimulus exposure time in the monkey. Arch. Psychiatr. Nervenkr. *222*, 281–291. https://doi.org/10.1007/BF00343237.

Chen, C.C., Bockisch, C.J., Bertolini, G., Olasagasti, I., Neuhauss, S.C.F., Weber, K.P., Straumann, D., and Ying-Yu Huang, M. (2014). Velocity storage mechanism in zebrafish larvae. J. Physiol. *592*, 203–214. https://doi.org/10.1113/jphysiol.2013.258640.

Cline, H. (2003). Sperry and Hebb: oil and vinegar? Trends Neurosci. *26*, 655–661. https://doi.org/10.1016/j.tins.2003.10.005.

Cohen, B., Henn, V., Raphan, T., and Dennett, D. (1981). Velocity storage, nystagmus, and visual-vestibular interactions in humans. Ann. N. Y. Acad. Sci. *374*, 421–433. https://doi.org/10.1111/j.1749-6632.1981.tb30888.x.

Darlington, C.L., and Smith, P.F. (2000). Molecular mechanisms of recovery from vestibular damage in mammals: recent advances. Prog. Neurobiol. *62*, 313–325. https://doi.org/10.1016/s0301-0082(00)00002-2.

De'sperati, C., Tempia, F., Harvey, R., and Strata, P. (1994). Vergence compensation during binocularly- and monocularly-evoked horizontal optokinetic nystagmus in the pigmented rat. Vis. Res. *34*, 3335–3345. https://doi.org/10.1016/0042-6989(94)90068-x.

Demer, J.L., and Robinson, D.A. (1983). Different time constants for optokinetic and vestibular nystagmus with a single velocity-storage element. Brain Res. *276*, 173–177. https://doi.org/10.1016/0006-8993(83)90560-7.

Dunn, T.W., Mu, Y., Narayan, S., Randlett, O., Naumann, E.A., Yang, C.T., Schier, A.F., Freeman, J., Engert, F., and Ahrens, M.B. (2016). Brain-wide mapping of neural activity controlling zebrafish exploratory locomotion. Elife *5*, e12741. https://doi.org/10.7554/eLife.12741.

Erickson, R.G., and Barmack, N.H. (1980). A comparison of the horizontal and vertical optokinetic reflexes of the rabbit. Exp. Brain Res. *40*, 448–456. https://doi.org/10.1007/BF00236153.

Fetter, M., and Zee, D.S. (1988). Recovery from unilateral labyrinthectomy in rhesus monkey. J. Neurophysiol. *59*, 370–393. https://doi.org/10.1152/jn.1988.59.2.370.

Furrow, R.E. (2019). Regression to the mean in pre-post testing: using simulations and permutations to develop null expectations. CBE Life Sci. Educ. *18*, le2. https://doi.org/10.1187/cbe.19-02-0034.

Gioanni, H., Rey, J., Villalobos, J., Bouyer, J.J., and Gioanni, Y. (1981). Optokinetic nystagmus in the pigeon (Columba livia). I. Study in monocular and binocular vision. Exp. Brain Res. *44*, 362–370. https://doi.org/10.1007/BF00238829.

Goc, G.L., Lafaye, J., Karpenko, S., Bormuth, V., Candelier, R., and Debrégeas, G. (2021). Thermal modulation of Zebrafish exploratory statistics reveals constraints on individual behavioral variability. BMC Biol. *19*, 208. https://doi.org/10.1186/s12915-021-01126-w.

Haffter, P., Granato, M., Brand, M., Mullins, M.C., Hammerschmidt, M., Kane, D.A., Odenthal, J., van Eeden, F.J., Jiang, Y.J., Heisenberg, C.P., et al. (1996). The identification of genes with unique and essential functions in the development of the zebrafish, Danio rerio. Development *123*, 1–36. https://doi.org/10.1242/dev.123.1.1.

Hess, B.J., Precht, W., Reber, A., and Cazin, L. (1985). Horizontal optokinetic ocular nystagmus in the pigmented rat. Neuroscience *15*, 97–107. https://doi.org/10.1016/0306-4522(85)90126-5.

Huang, Y.Y., and Neuhauss, S.C.F. (2008). The optokinetic response in zebrafish and its applications. Front. Biosci. *13*, 1899–1916. https://doi.org/10.2741/2810.

Huang, Y.Y., Rinner, O., Hedinger, P., Liu, S.C., and Neuhauss, S.C.F. (2006). Oculomotor instabilities in zebrafish mutant belladonna: a behavioral model for congenital nystagmus caused by axonal misrouting. J. Neurosci. *26*, 9873–9880. https://doi.org/10.1523/JNEUROSCI.2886-06.2006.

Huber-Reggi, S.P., Chen, C.C., Grimm, L., Straumann, D., Neuhauss, S.C.F., and Huang, M.Y.Y. (2012). Severity of infantile nystagmus syndrome-like ocular motor phenotype is linked to the extent of the underlying optic nerve projection defect in zebrafish belladonna mutant. J. Neurosci. *32*, 18079–18086. https://doi.org/10.1523/JNEUROSCI.4378-12.2012.

Igarashi, M., Isago, H., and Alford, B.R. (1983). Effects of prolonged optokinetic stimulation on oculomotor and locomotor balance functions. Acta Otolaryngol. *95*, 560–567. https://doi.org/10.3109/00016488309139443.

Jareonsettasin, P., Otero-Millan, J., Ward, B.K., Roberts, D.C., Schubert, M.C., and Zee, D.S. (2016). Multiple time courses of vestibular set-point Adaptation revealed by sustained magnetic field stimulation of the labyrinth. Curr. Biol. *26*, 1359–1366. https://doi.org/10.1016/j.cub.2016.03.066.

Johnston, A.R., Him, A., and Dutia, M.B. (2001). Differential regulation of GABA(A) and GABA(B) receptors during vestibular compensation. Neuroreport *12*, 597–600. https://doi.org/10.1097/00001756-200103050-00033.

Keng, M.J., and Anastasio, T.J. (1997). The horizontal optokinetic response of the goldfish. Brain Behav. Evol. *49*, 214–229. https://doi.org/10.1159/000112993.

Klar, M., and Hoffmann, K.P. (2002). Visual direction-selective neurons in the pretectum of the rainbow trout. Brain Res. Bull. *57*, 431–433. https://doi.org/10.1016/s0361-9230(01)00706-7.

Lambert, F.M., Beck, J.C., Baker, R., and Straka, H. (2008). Semicircular canal size determines the developmental onset of angular vestibuloocular reflexes in larval Xenopus. J. Neurosci. *28*, 8086–8095. https://doi.org/10.1523/JNEUROSCI.1288-08.2008.

Laurens, J., and Angelaki, D.E. (2011). The functional significance of velocity storage and its dependence on gravity. Exp. Brain Res. *210*, 407–422. https://doi.org/10.1007/s00221-011-2568-4.

Leigh, R.J., Robinson, D.A., and Zee, D.S. (1981). A hypothetical explanation for periodic alternating nystagmus: instability in the optokinetic-vestibular system. Ann. N. Y. Acad. Sci. *374*, 619–635. https://doi.org/10.1111/j.1749-6632.1981.tb30906.x.

Lim, R., Callister, R.J., and Brichta, A.M. (2010). An increase in glycinergic quantal amplitude and frequency during early vestibular compensation in mouse. J. Neurophysiol. *103*, 16–24. https://doi.org/10.1152/jn.91223.2008.

Lin, T.F., Mohammadi, M., Fathalla, A.M., Pul, D., Lüthi, D., Romano, F., Straumann, D., Cullen, K.E., Chacron, M.J., and Huang, M.Y.Y. (2019). Negative optokinetic afternystagmus in larval zebrafish demonstrates set-point adaptation. Sci. Rep. *9*, 19039. https://doi.org/10.1038/s41598-019-55457-4.

Maioli, C. (1988). Optokinetic nystagmus: modeling the velocity storage mechanism. J. Neurosci. *8*, 821–832.

Mueller, K.P., and Neuhauss, S.C.F. (2010). Quantitative measurements of the optokinetic response in adult fish. J. Neurosci. Methods *186*, 29–34. https://doi.org/10.1016/j.jneumeth.2009.10.020.

Naganathan, S.R., Popovic, M., and Oates, A.C. (2022). Left-right symmetry of zebrafish embryos requires somite surface tension. Nature *605*, 516–521. https://doi.org/10.1038/s41586-022-04646-9.

Nelson, A.B., Faulstich, M., Moghadam, S., Onori, K., Meredith, A., and du Lac, S. (2017). BK channels are required for multisensory plasticity in the oculomotor system. Neuron *93*, 211–220. https://doi.org/10.1016/j.neuron.2016.11.019.

Neverov, V.P., Buresová, O., and Bures, J. (1977). Effect of ECS on the neural traces underlying the reversive postoptokinetic nystagmus in the rabbit. Physiol. Behav. *18*, 7–11. https://doi.org/10.1016/0031-9384(77)90085-3.

Pérez-Schuster, V., Kulkarni, A., Nouvian, M., Romano, S.A., Lygdas, K., Jouary, A., Dipoppa, M., Pietri, T., Haudrechy, M., Candat, V., et al. (2016). Sustained rhythmic brain activity underlies visual motion perception in zebrafish. Cell Rep. *17*, 3089. https://doi.org/10.1016/j.celrep.2016.12.007.

Qian, H., Zhu, Y., Ramsey, D.J., Chappell, R.L., Dowling, J.E., and Ripps, H. (2005). Directional asymmetries in the optokinetic response of larval zebrafish (Danio rerio). Zebrafish *2*, 189–196. https://doi.org/10.1089/zeb.2005.2.189.

Qian, Z., Micorescu, M., Yakhnitsa, V., and Barmack, N.H. (2012). Climbing fiber activity reduces 14-3-3-theta regulated GABA(A) receptor phosphorylation in cerebellar Purkinje cells. Neuroscience *201*, 34–45. https://doi.org/10.1016/j.neuroscience.2011.11.021.

Shawkat, F.S., Harris, C.M., and Taylor, D.S. (2001). Spontaneous reversal of nystagmus in the dark. Br. J. Ophthalmol. *85*, 428–431. https://doi.org/10.1136/bjo.85.4.428.

Vibert, N., Beraneck, M., Bantikyan, A., and Vidal, P.P. (2000). Vestibular compensation modifies the sensitivity of vestibular neurones to inhibitory amino acids. Neuroreport *11*, 1921–1927. https://doi.org/10.1097/00001756-200006260-00023.

Waespe, W., Cohen, B., and Raphan, T. (1985). Dynamic modification of the vestibulo-ocular reflex by the nodulus and uvula. Science *228*, 199–202. https://doi.org/10.1126/science.3871968.

Waespe, W., and Henn, V. (1977). Vestibular nuclei activity during optokinetic after-nystagmus (OKAN) in the alert monkey. Exp. Brain Res. *30*, 323–330. https://doi.org/10.1007/BF00237259.

Waespe, W., and Henn, V. (1978). Reciprocal changes in primary and secondary optokinetic after-nystagmus (OKAN) produced by repetitive optokinetic stimulation in the monkey. Arch. Psychiatr. Nervenkr. *225*, 23–30. https://doi.org/10.1007/BF00367349.

Waespe, W., Huber, T., and Henn, V. (1978). Dynamic changes of optokinetic after-nystagmus (OKAN) caused by brief visual fixation periods in monkey and in man. Arch. Psychiatr. Nervenkr. *226*, 1–10. https://doi.org/10.1007/BF00344118.

Waespe, W., and Wolfensberger, M. (1985). Optokinetic nystagmus (OKN) and optokinetic after-responses after bilateral vestibular neurectomy in the monkey. Exp. Brain Res. *60*, 263–269. https://doi.org/10.1007/BF00235920.

Wallman, J. (1993). Subcortical optokinetic mechanisms. Rev. Oculomot. Res. *5*, 321–342.

Wallman, J., and Velez, J. (1985). Directional asymmetries of optokinetic nystagmus: developmental changes and relation to the accessory optic system and to the vestibular system. J. Neurosci. *5*, 317–329.

Wu, Y., Dal Maschio, M., Kubo, F., and Baier, H. (2020). An optical illusion pinpoints an essential circuit node for global motion processing. Neuron *108*, 722–734.e5. https://doi.org/10.1016/j.neuron.2020.08.027.

Xie, J., Jusuf, P.R., Bui, B.V., and Goodbourn, P.T. (2019). Experience-dependent development of visual sensitivity in larval zebrafish. Sci. Rep. *9*, 18931. https://doi.org/10.1038/s41598-019-54958-6.

Yokota, J., Reisine, H., and Cohen, B. (1992). Nystagmus induced by electrical stimulation of the vestibular and prepositus hypoglossi nuclei in the monkey: evidence for site of induction of velocity storage. Exp. Brain Res. *92*, 123–138. https://doi.org/10.1007/BF00230389.

Yucel, Y.H., Kim, M.S., Jardon, B., and Bonaventure, N. (1990). Abolition of monocular optokinetic nystagmus directional asymmetry after unilateral visual deprivation in adult vertebrates: involvement of the GABAergic mechanism. Brain Res. Dev. Brain Res. *53*, 179–185. https://doi.org/10.1016/0165-3806(90)90004-i.

Zee, D.S., Jareonsettasin, P., and Leigh, R.J. (2017). Ocular stability and set-point adaptation. Philos. Trans. R. Soc. Lond. B Biol. Sci. *372*, 20160199. https://doi.org/10.1098/rstb.2016.0199.

STAR★METHODS

KEY RESOURCES TABLE

REAGENT or RESOURCE	SOURCE	IDENTIFIER
Deposited data		
Data repository	This paper	https://data.mendeley.com/datasets/wgyyp4jw5w/1
Mathematical model repository	This paper	https://github.com/tingfenglin-ac/Optokinetic-set-point-adaptation-model
Experimental models: Cell lines		
Zebrafish: TU	European Zebrafish Resource Center	Cat: 1173
Software and algorithms		
LabVIEW	National Instruments, Austin, Texas, USA	N/A
MATLAB	MathWorks, Natick, MA, USA	N/A

RESOURCE AVAILABILITY

Lead contact

Further information and requests about this study should be directed to and will be fulfilled by the lead contact, Ting-Feng Lin (tingfenglin.ac@gmail.com).

Materials availability

This study did not generate new unique reagents.

Data and code availability

- Data presented in this study are saved as MAT-file (version 7.0) and publicly available from Mendeley Data: https://data.mendeley.com/datasets/wgyyp4jw5w/1.
- The code of the mathematical model is written in MATLAB R2020a and publicly available from GitHub: https://github.com/tingfenglin-ac/Optokinetic-set-point-adaptation-model.
- Any additional information required to reanalyze the data reported in this paper is available from the lead contact upon request.

EXPERIMENTAL MODEL AND SUBJECT DETAILS

Larval zebrafish

In accordance with the Federal Veterinary Office of Switzerland (FVO) guidelines - TSchV art. 112, no ethical approval is required for studies on larvae under the age of 120 h/5 days post fertilization prior to the independent feeding. Zebrafish embryos of TU wild-type zebrafish line were bred and maintained in 28°C E3 solution (5 mM NaCl, 0.17 mM KCl, 0.33 mM CaCl2, and 0.33 mM MgSO4) (Haffter et al., 1996) under a cycle of 14 h of light and 10 h of darkness. Larvae at the age of 5 days postfertilization were used for the experiments.

METHOD DETAILS

Visual stimulation

To minimize the influence of circadian rhythms on zebrafish behavior, all experiments were performed between 8:00 AM and 7:00 PM. Zebrafish larvae were restrained with low-melting agarose (Sigma Type VII-A) in the center of an optokinetic cylinder without immobilizing the eyes (Arrenberg, 2016). OKN was evoked through the use of four digital light projectors (Samsung SP-H03 Pico Projector). The optokinetic stimulus consisted of a moving, computer-controlled black and white vertical sinusoid grating pattern with a spatial frequency of 0.053 cycles per degree and 100% contrast (maximum illumination 1524 lux) projected onto a transparent screen at angular velocities depending on the experimental conditions. A custom program written in LabVIEW (National Instruments, Austin, Texas, USA) (Chen et al., 2014) was used to control all

experimental processes and conditions, including frame processing, data recording, visual stimulus properties, and illumination.

Stimulus procedure

Throughout this study, prestimulatory eye movements were recorded in darkness for 5 min. Unidirectional optokinetic stimulation in 10 deg/sec was given for 10 min followed by 10 min of poststimulatory darkness, respectively. An alternating stimulation paradigm consisted of two sessions of stimulatory phases interspersed with pre-, inter- and poststimulatory phases. Prestimulatory eye movements were recorded in 5 min of darkness followed by 20 min of direction-alternating moving grating, i.e., the first stimulatory phase. After the first stimulatory phase, the aftereffect was tested in the dark for 5 min (the interstimulatory phase), and then alternating stimulation was given for another 20 min (the second stimulatory phase). After the second session of alternating stimulation, the recording continued for 10 min in darkness (the poststimulatory phase). During both symmetric (10 deg/sec in both directions; 10/10 SA stimulation) and asymmetric (20 or 10 deg/sec in one direction and 5 deg/sec in the other direction; 20/5 and 10/5 AA stimulations) alternating optokinetic stimulation, a cycle of a 15-s stimulus in one direction followed by a 15-s stimulus in the other direction was repeated for the entire 20-min stimulatory phase (Figure 1C). The starting direction of the stimulus was random.

Eye movement recording and analysis

Zebrafish larvae at the age of 5 days postfertilization were chosen and tested. The restrained larva was illuminated from below with infrared (IR)-emitting diodes (λpeak = 875 ± 15 nm, OIS-150 880, OSA Opto Light GmbH, Germany). The eye movements were recorded at a sampling rate of 40 frame/second by an IR-sensitive charge-coupled device (CCD) camera. The area around the eyes was manually selected as the region of interest. Data were analyzed using custom-developed programs written in MATLAB (MathWorks, Natick, Massachusetts, USA). Eye-position traces were smoothed using a Gaussian filter with a cutoff frequency of 5.5 Hz. Eye movement velocity was calculated as the derivative of the eye-position traces. The SPV was estimated as the median velocity in the first second of each slow phase after discarding the quick-phase eye movement. Quick-phase eye movement was first selected by an algorithm with a velocity threshold of 20 deg/sec and an eye dislocation threshold of 1 deg, after which the cursor was manually adjusted if necessary. Population median was obtained from the average SPV of every 1-s time bin in every individual fish. In this study, we collected data from both eyes, under the assumption that the inherent T-N asymmetry of the optokinetic system in lateral-eyed animals (Bonaventure et al., 1983; Braun and Gault, 1969; De'sperati et al., 1994; Erickson and Barmack, 1980; Gioanni et al., 1981; Hess et al., 1985; Huang and Neuhauss, 2008; Keng and Anastasio, 1997; Klar and Hoffmann, 2002; Mueller and Neuhauss, 2010; Qian et al., 2005; Wallman, 1993; Wallman and Velez, 1985; Yucel et al., 1990) may lead to different results for each eye.

Model

We used the model from our previous study (Lin et al., 2019) to explain how set-point adaptation as well as negative OKAN are induced during asymmetric stimulation. During stimulus presentation, retinal slip, $V_r(t)$, is computed by comparing the eye velocity, $V_e(t)$, to stimulus velocity, $V_s(t)$, as $V_r(t) = V_s(t) - V_e(t)$, and is fed into a habituation leaky integrator which captures habitation in retinal ganglion cells and downstream areas (Perez-Schuster et al., 2016) (Figure 3A). As the previous model has been used to predict the behavior under a unidirectional stimulation, in order to preserve the proposed function of each operator under the direction-alternating stimuli, here, we adapted the model according to the new stimuli. In particular, we added an absolute value function and corrected the sign of the habituated retinal slip velocity signal accordingly, as the habituation of the signal does not depend on the direction in which the stimulus is moving (see Figure 4Ai by Pérez-Schuster et al. (Perez-Schuster et al., 2016)). Thus, the output of the habituation integrator, $H(t)$, is described by

$$\frac{dH(t)}{dt} = -\frac{1}{T_h}H(t) + \frac{k_h}{T_h}|V_r(t)| \qquad \text{(Equation 1)}$$

where $V_r(t)$ denotes retinal slip velocity, $|.|$ denotes absolute value operator, and k_h and T_h denote habituation integrator gain and time constant, respectively. Our behavioral data demonstrates asymmetric nasal and temporal gains consistent with previous studies (Huang and Neuhauss, 2008; Mueller and Neuhauss, 2010; Qian et al., 2005) which are captured via a piecewise linear function whose value depends on whether the eye is moving in a nasalward or temporalward direction. Nasal/temporal gains are calculated from data

by averaging and scaling the eye velocity during nasal/temporal eye movement (see Table S1). The filtered retinal slip signal, $V_f(t)$, is then computed as following:

$$V_f(t) = g_{T/N}(hV_r(t) - sign(V_r(t))H(t)) \quad \text{(Equation 2)}$$

where $sign(.)$ is the sign function, and h and $g_{T/N}$ are habituation and temporal/nasal gain, respectively. $V_f(t)$, together with the internal setpoint signal (the output of the adaptation integrator), $A(t)$, is compared to define an error signal, $E(t) = V_f(t) - A(t)$, that drives the oculomotor motor system in order to match the eye movement to stimulus as $V_e(t) = gE(t) + Q(t)$ in which $Q(t)$ is the output of the velocity storage integrator and g is the oculomotor gain. Moreover, $Q(t)$ and $A(t)$ are computed by solving the following differential equations:

$$\frac{dQ(t)}{dt} = -\frac{1}{T_{vsm}}Q(t) + \frac{k_{vsm}}{T_{vsm}}E(t) \quad \text{(Equation 3)}$$

$$\frac{dA(t)}{dt} = -\frac{1}{T_a}A(t) + \frac{k_a}{T_a}V_e(t) \quad \text{(Equation 4)}$$

where k_a, T_a, k_{vsm}, and T_{vsm} denote adaptation gain, adaptation time constant, velocity storage gain, and velocity storage time constant, respectively. During darkness, V_f is zero and therefore, the error signal is solely defined by inverting the sign of the setpoint value. Equations 1, 3 and 4 constitute a system of ordinary differential equation with three variables, $H(t)$, $A(t)$, and $Q(t)$ which were solved using *ode*45 function in MATLAB for a given set of parameters (i.e., time constants and gains).

Parameter estimation

To estimate the parameters (i.e., k_a, T_a, k_{vsm}, T_{vsm}, k_h, T_h, g, and h) of the model for a given stimulation condition, we used the system identification toolbox in MATLAB. We used nonlinear least square method and trust-region algorithm with fixed time steps of 0.1 to find a set of parameters that maximize variance-accounted-for (VAF) for our model:

$$VAF = \left(1 - \frac{var(V_{e,model} - V_{e,measured})}{V_{e,measured}}\right) \times 100\ \% \quad \text{(Equation 5)}$$

where $V_{e.model}$ and $V_{e,measured}$ denote simulated and experimental values and $var(.)$ denotes variance. A model with a perfect fit yields a VAF value of 100%, whereas any deviation of the simulated model from the experimental data results in VAF values less than 100%.

For median population behavior, we chose the data from 10/10 SA stimulus condition to estimate the parameters of the model. Each stimulation protocol includes 5 min of darkness followed by two stimulatory phases. The first stimulatory phase consists of 20 min of stimulus followed by 5 min of darkness. The second stimulatory phase consists of 20 min of stimulus followed by 10 min of darkness. We estimated the parameters of the model by using the data from one stimulatory phase and tested the performance of the model by using the data from the other. Specifically, we built the first model by using the data from the first stimulatory phase, then tested and validated the model by using the data from the second stimulatory phase. Similarly, we built the second model by using the data from the second stimulatory phase, then tested and validated the model by using the data from the first stimulatory phase. Regardless, both models resulted in qualitatively and quantitively similar performance. Also, the parameters were similar in both cases (Table S2). In all the representative simulations, we only predict the behaviors by using the first model.

When validating the model, we used the same parameters for all conditions, but $g_{T/N}$, the temporal/nasal gain. Specifically, $g_{T/N}$ is estimated separately for each stimulus condition (Table S1) by scaling the average SPV during OKN (i.e., colored circles in Figures S3C, S3F, and S3I). After estimating the parameters using the data from a given stimulus condition, we quantified the goodness of fit for each stimulus condition. Here, we report the parameters estimated and tested using symmetric +/− 10 deg/s stimulus and validated by +20/-5 and +10/-5 deg/s stimulus (Table S2). Qualitatively similar results were obtained when using other stimulus conditions for parameter estimation (data not shown).

Finally, we show that introducing an internal bias to the model can explain observed adaptation and negative OKAN seen in symmetric stimulation condition for particular individual fish (Figure 5A). The parameters of the model for individual fish were the same as that of the median population, except $g_{T/N}$ for each fish

was computed individually by scaling the average SPV during OKN (i.e., black dots in Figure S3C). Furthermore, the value of bias, *B*, was estimated for each fish.

The parameters estimated here (Table S1) are consistent with those obtained in our previous paper (Lin et al., 2019). An exception is the habituation time constant (T_h); Our sensitivity and optimization analysis showed that a higher value of T_h could explain the behavior more robustly in which case the simulation results are well generalizable. This could be due to nonlinearity introduced through absolute value and sign operators which could influence pole-zero displacement differentially.

QUANTIFICATION AND STATISTICAL ANALYSIS

Statistical analysis

We collected data from a total of 29 (10/10 SA group), 21 (10/5 AA group), and 18 (20/5 AA group) larval zebrafish for our experiments. All statistical analyses were performed using MATLAB. The trace representing the general SPV of each group is shown as median $\pm$ median absolute deviation (MAD). Pearson correlation was used to estimate the linear relationship. Correlation coefficients (R) and P-value (p) are provided in each scatter plot to show the relationship between two measures. Linear regression represents the response of the ordinary least-squares fit of the data. To compare two slopes, interactive analysis of the covariance and the post hoc Tukey's method were applied. All graphs of Gaussian function were plotted according to the mean and standard deviation of the ΔSPV. To compare the nasalward and temporalward SPVs of two eyes, we averaged the SPV in each direction throughout the alternating stimulation of each individual larva. To determine the significance of the difference between nasalward and temporalward SPV, means $\pm$ standard deviations were computed and paired-sample t-test was performed.

Randomization test

To demonstrate the set-point adaptation during symmetric stimulation, we plotted the gradual change in ΔSPV over stimulation (Figures S4A–S4D). However, regression toward the mean as a statistical phenomenon may mislead us on interpreting our data. To avoid such misinterpretation, Furrow suggested that one can generate a null expectation by using the permutations of the original data (Furrow, 2019). Considering the low feasibility and the unnecessity to include all possible permutations of the 40-min time series data, we only analyzed 1000 different permutations that were obtained by randomly shuffling every 30-s bin of the original data (1000 permutations of the original data from each fish for a total of 29 fish). Within each 30-s bin, stimuli in both directions are included (15 s for each direction). Considering the shuffling would wipe out the effect of the temporal integration, we expect to see random changes rather than a consistent trend of ΔSPV in permutations over time. As expected, without the correct temporal order in the shuffled data, the gradual change in ΔSPV is diminished (Figures S4E–S4H). In addition to the empirical data, the same shuffling strategy was also applied to the simulated data obtained from our mathematical model (Figure S5). To statistically test the compensating effect caused by set-point adaptation, the analyses of the original data were statistically compared to the analyses of the shuffled data (Figures 4I–4J and 6H–6I).